5.3 THE ORGANIZATION OF OCEANIC CONVECTION DURING THE ONSET OF THE EAST ASIAN SUMMER MONSOON

Richard H. Johnson* and Steven L. Aves
Colorado State University, Fort Collins, Colorado

1. INTRODUCTION

It has long been known that the organization of tropical convection is influenced predominantly by the vertical shear and convective available potential energy or CAPE (e.g., Moncrieff and Green 1972). Various observational studies in the eastern Atlantic and northern Australia have confirmed the strong influence of environmental winds and CAPE on the structure and orientation of convective bands (e.g., Barnes and Seickman 1984; Alexander and Young 1992; Keenan and Carbone 1992). Recently, LeMone et al. (1998) investigated the organization of convection over the western Pacific warm pool using aircraft data from TOGA COARE. They found that vertical shear in the low-to-midtroposphere was key in determining the orientation of convective bands, while CAPE influenced their depth and longevity. Their results have been recently supported by numerical simulations of convection in shear by Robe and Emanuel (2001).

The way in which convection organizes is important from several perspectives. First, it has an important effect on the vertical distribution of heating. For example, it is well known that convection that organizes perpendicular to the low-level shear vector often produces squall lines with extensive stratiform precipitation (Houze 1977; Zipser 1977), and that the corresponding latent heating profiles for the convective and stratiform components of squall systems can be quite different (Houze 1982; Johnson 1984). Systems containing extensive stratiform precipitation have quite different heating profiles from those which consist principally of deep convection. In addition, there is evidence to suggest that convective momentum transport is a function of system organization, with up-gradient transport in the line-normal direction and down-gradient transport in the line-parallel direction (LeMone 1983; Wu and Yanai 1994; Tung and Yanai 2002). Further, observations from COARE indicate that surface fluxes are greatly enhanced in convection that is highly organized and contains extensive stratiform precipitation areas as opposed to less-organized convective systems (Saxen and Rutledge 1998). Finally, the extent of high clouds and cirrus associated with convective systems may depend on their organization, which would then influence the surface and tropospheric radiative fluxes.

*Corresponding author address: Richard H. Johnson, Department of Atmospheric Science, Colorado State University, Fort Collins, CO 80523-1371; johnson@atmos.colostate.edu

2. DATA AND ANALYSIS PROCEDURES

Ground-based radar data are obtained from the BMRC, 5-cm dual-polarimetric Doppler radar (C-POL) that was located at Dongsha Island in the northern SCS (Fig. 1). C-POL was operational from May 4 to June 21 with several days of data gaps. However, the dataset is complete for the period of this study, 15–25 May. Animations of the C-POL radar base-scan reflectivity within ∼200 km radius of Dongsha Island were used to determine the dominant modes of convective organization at six-hour intervals (e.g., 03–09, 09–15 UTC, etc.). Lines were classified as shear-parallel (or shear-perpendicular) if the line orientations were within 30° of specific shear vectors (or their perpendicular components) for the low- and midtroposphere. Eight-hundred to 400 hPa was selected as the nominal midlevel shear layer; however, there were some instances where shear-parallel bands were more closely aligned along the shear vector for slightly different layers, e.g., 700–400 hPa, 800–500 hPa, etc. Therefore, in practice, bands were defined as shear-parallel if they were within 30° of the shear vector for a layer 300 or 400-hPa deep between 800 and 400 hPa. In addition, since the vertical shear likely varied horizontally over the radar domain on many occasions, selection of bands for classification was done as often as possible in proximity to the sounding site used for the analysis at *Shiyan 3* (Fig. 1). As might be expected, classification of bands was not always unambiguous; however, in most instances the choices were reasonably clear.

The fields of radar reflectivity were partitioned into convective and stratiform components using the procedure of Steiner et al. (1995), with modifications to correct the misassignment of some convective cells as stratiform rainfall as described in Aves and John-

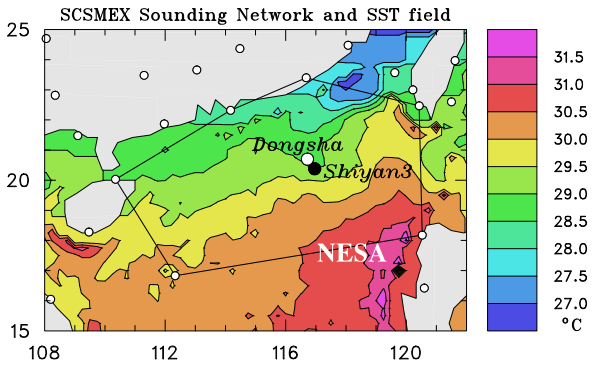

Figure 1: SCSMEX/GAME sounding network, SST distribution (scale to right), and Northern Enhanced Sounding Array (NESA) for May-June 1998. BMRC C-POL radar was on Dongsha Island, and soundings used in study were from R/V *Shiyan 3*.

son (2003).

The mean SST field (Fig. 1) was derived from daily values obtained from the TRMM Microwave Imager (TMI) SST product (Wentz et al. 2000). The C-POL radar on Dongsha Island was located 40 km northwest of R/V *Shiyan 3*, where six-hourly Vaisala-GPS soundings were launched. The *Shiyan 3* soundings, rather than those at Dongsha Island, are used as proximity soundings for the convection in the C-POL radar range since a single sounding type was used there (two sounding systems were used at Dongsha). The sounding polygon in Fig. 1 is referred to as the Northern Enhanced Sounding Array or NESA. Sounding quality control procedures and other aspects of the sounding data analysis are described in Johnson and Ciesielski (2002).

3. SUMMARY OF MODES OF ORGANIZATION

Four primary modes of organization have emerged from the results of this study, which are summarized in Fig. 2.

This figure, adapted from LeMone et al. (1998), is a summary of their findings from TOGA COARE, but supplemented by new results from SCSMEX (two new modes **2r**, and **4c**). In general, the organizational modes for SCSMEX were consistent with those determined by LeMone et al. (1998) for the western Pacific warm pool. They found that when the shear in the lowest 200 hPa exceeded 4 m s^{-1} and the shear from 800 to 400 hPa was less than 5 m s^{-1}, the orientation of primary convective band was perpendicular to the low-level shear (Type **2** in Fig. 2). Secondary lines parallel to the low-level

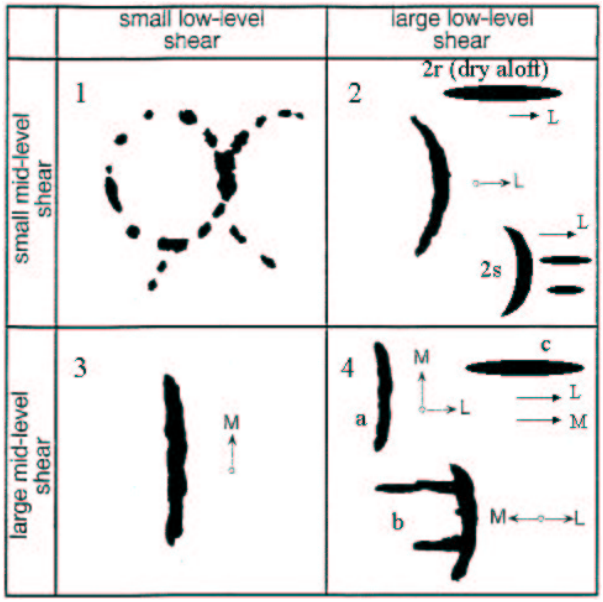

Figure 2: Schematic depiction from LeMone et al. (1998) of convective structures for given vertical shears in the lower troposphere (1000–800 hPa) and at middle levels (800–400 hPa) based on COARE observations, but modified to include results from SCSMEX. Length of schematic convective bands is ∼100–300 km; line segments in upper-left frame are up to 50 km length. Cutoff between "strong" and "weak" shear for lower layer (1000–800 hPa) is 4 m s^{-1} and for middle layer (800–400 hPa) is 5 m s^{-1}. Arrows marked **L** and **M** are shear vectors for lower and middle layers, respectively.

shear were found in some cases ahead of the primary band (not shown in their figure, but included here as **2s** in Fig. 2). In the absence of strong low-level shear, lines formed parallel to the 800-400 hPa shear when its magnitude exceeded 5 m s^{-1} (**3** in lower-left frame). When the vertical shear exceeded the thresholds in both layers and the shear vectors were not in the same direction (lower-right frame), the primary band was normal to the low-level shear (**4a** or **4b**). Trailing secondary bands parallel to the midlevel shear occurred if the midlevel shear was opposite the low-level shear (**4b**). When the shear in both layers was weak, convection developed in arcs along outflow boundaries (**1**). Two additional modes of convection have been identified from analysis of SCSMEX C-POL radar data (Fig. 2): shear-parallel bands (**2r**) for strong low-level shear and weak midlevel shear when the air is dry aloft, and shear-parallel bands (**4c**) for strong shears in both layers when the shear vectors are in the same direction.

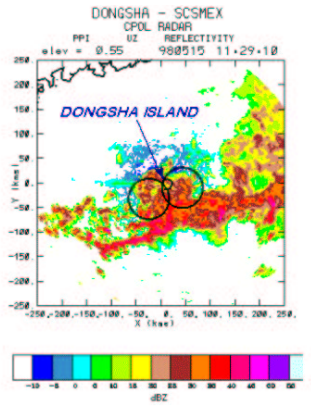

Figure 3: Radar reflectivity (dBZ) from C-POL radar on Dongsha Island for 1129 UTC 15 May 1998. Intersecting circles are dual-Doppler lobes for C-POL and TOGA radar (on *Shiyan 3*). At this time the surface wind at Dongsha shifted to northeasterly and the temperature dropped by 4°C.

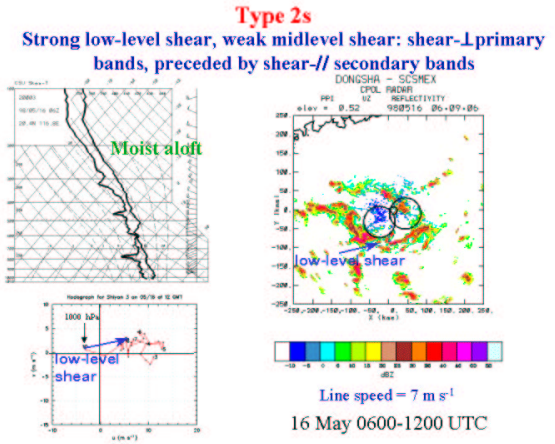

Figure 4: *Shiyan 3* sounding (upper left) and hodograph (lower left) at 0600 UTC, and C-POL radar reflectivity (right) at 0609 UTC on 16 May 1998 for Type **2s** case (strong low-level shear, weak midlevel shear, moist aloft: shear-perpendicular primary bands preceded by shear-parallel secondary bands).

4. A FEW ILLUSTRATIVE CASES

The first significant convection occurred on 15 May, but it was influenced by a frontal system that moved south from the southern China coast, leading to a temperature drop of 4°C and shift to northerly wind at Dongsha Island. The convective band associated with the front can be seen in Fig. 3. The frontal contrast may have been aided by convergence in the region of north-south SST gradient (Fig. 1), a frontogenetic situation. Convection after the 15th was mostly nonfrontal, although a shift to northerly wind and some cooling occurred again on 19 May. In order to concentrate primarily on nonfrontal convection, classification of precipitation systems was restricted to the period 16–25 May.

Because the low-level flow was relatively strong throughout the period, only two cases of weak-shear events were observed (**1**'s in Fig. 2). In these instances, convection was observed to develop in arcs along outflow boundaries.

Three varieties of the Type **2** classification were observed during SCSMEX (strong low-level shear, weak midlevel shear). Only two cases had shear-perpendicular primary bands, one with preceding shear-parallel secondary bands (**2s**) and one without (**2**). The **2s** case (16 May) is shown in Fig. 4.

The low-level shear vector taken from the hodograph has been placed on the reflectivity plot. There appear to be several primary bands quasi-perpendicular to the low-level shear vector, while several bands are ahead nearly parallel to it. The primary bands moved to the east-northeast at 7 m s^{-1}. The sounding shows moderate instability (average CAPE for three soundings centered on this time was 1248 J kg^{-1}) and moist conditions in the upper troposphere.

By way of contrast, Type **2r** convection developed at a time of dry conditions aloft (Fig. 5). Weak convective lines (reflectivities < 40 dBZ) developed approximately parallel to the low-level shear vector. The spacing of these bands (∼50 km) is much greater than the boundary layer depth, much like the cloud lines found by LeMone and Meitin (1984) in the trade wind boundary layer off Puerto Rico. Of course, additional rows of nonprecipitating clouds could have existed between the bands in Fig. 5. Such features, referred to as *wide mixed-layer rolls* by Young et al. (2002), to distinguish them from *narrow mixed-layer rolls* associated with individual longitudinal roll vortices, have been attributed to a variety of mechanisms, as summarized by Chlond (1988): anisotropy in eddy fluxes of heat and momentum, poor thermal conductivity at the top of the boundary layer, large-scale sinking motions, and latent heat release. However, there is no general consensus on the mechanisms for these wide mixed-layer rolls. The occurrence of precipitation (from congestus clouds) in these bands indicates that latent heat release may have been a factor in the wide spacing of the bands. The dry air aloft (upper-left panel, Fig. 5) that capped the congestus clouds at this time was associated with subsidence and northwesterly flow following the passage of an upper-level trough.

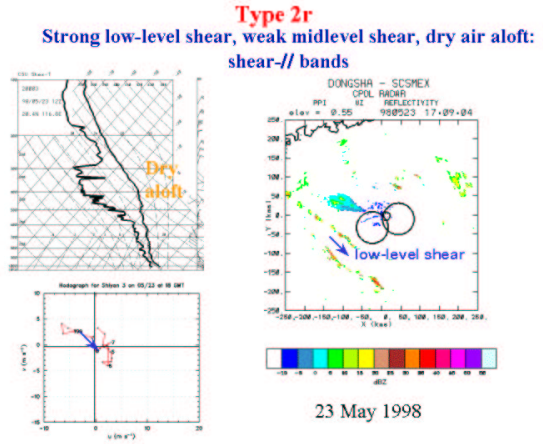

Figure 5: *Shiyan 3* sounding (upper left) and hodograph (lower left) at 1200 UTC, and C-POL radar reflectivity (right) at 1709 UTC on 23 May 1998 for Type **2r** case (strong low-level shear, weak midlevel shear, dry aloft: weak shear-parallel bands).

For the sake of brevity, we will omit depictions of the remaining modes.

5. SUMMARY OF MODES IN RELATION TO SHEAR

Time series of the vertical shears in the lower (1000–800 hPa) and middle (800–400 hPa) troposphere at *Shiyan 3* for 13–28 May are shown in Fig. 6. There is an overall trend toward decreasing midlevel shear and increasing low-level shear as the transition to summer occurred – the midlevel jet shifted northward and the low-level monsoon flow strengthened. However, there was also considerable high-amplitude, short-term variability in the shear, which accounted for a surprisingly large variety of convective systems in this region on short time scales. Shading in Fig. 6 denotes periods when the shear exceeded thresholds defined by LeMone et al. (1998) for the specific organizational modes of convection. Layer shear directions, used to classify line orientations, were computed but are not shown in Fig. 6.

From Fig. 6 (second panel) it is evident that a slightly greater number of shear-parallel convective bands than shear-perpendicular bands occurred over the northern SCS during the early monsoon onset period of SCSMEX. The results show that, in general, shear-perpendicular convection was common when the low-level shear exceeded 4 m s^{-1}. This finding is consistent with the idea that convection organizes to establish a balance between the cold pool and low-level shear when the low-level shear is

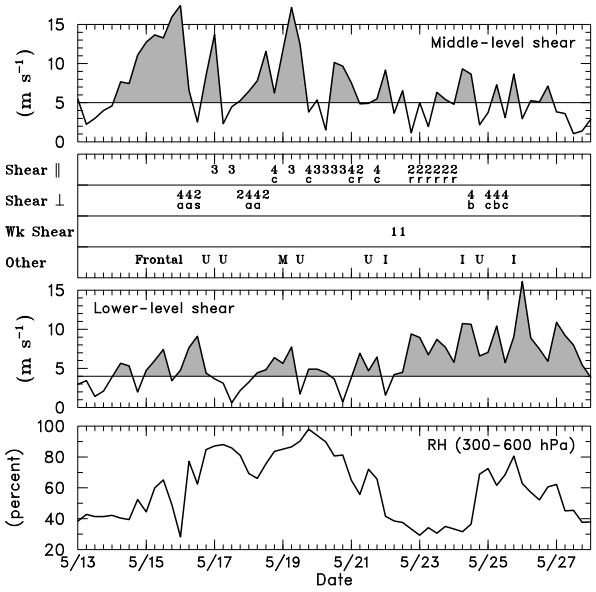

Figure 6: Time series of shear vector magnitude in the low levels (1000–800 hPa) and middle levels (800–400 hPa), and 600–300 hPa relative humidity, based on six-hourly sounding data from *Shiyan 3*. Periods with shear exceeding 5 m s^{-1} in the middle levels and 4 m s^{-1} in the lower levels are shaded. Convective organization in relation to the shear in the two layers indicated in second panel from top, with numbers and letters referring to organizational modes depicted in Fig. 1. Those cases not fitting any of those modes are denoted as **Other**: **Frontal** = convection influenced by frontal system; **U** = Unclassifiable; **I** = Isolated convection; **M** = Missing.

sufficiently large (Rotunno et al. 1988). An exception occurred on 23 May when the midtroposphere became extremely dry (as seen in the 300–600 hPa mean relative humidity time series, lower panel, Fig. 6), thus preventing deep convection and their associated downdrafts and leading to shallow, shear-parallel lines. These lines are indicated by **2r** in Fig. 6, where **r** indicates convection likely associated with longitudinal roll vortices in the boundary layer (Kuettner 1971; LeMone 1973; Christian and Wakimoto 1989). Isolated convective cells (**I**) also occurred during this period, likely due to a suppression of deep convection by the dry air aloft.

Most of the shear-perpendicular bands during SCSMEX were of the **4** variety since midlevel shear was also generally strong, although three **2**'s also occurred. This control on convective organization was influenced by the proximity of SCSMEX to the midlatitude westerlies, although this influence declined later in the period. With strong westerly shears at both low- and midlevels during this period, shear-parallel bands developed on four occa-

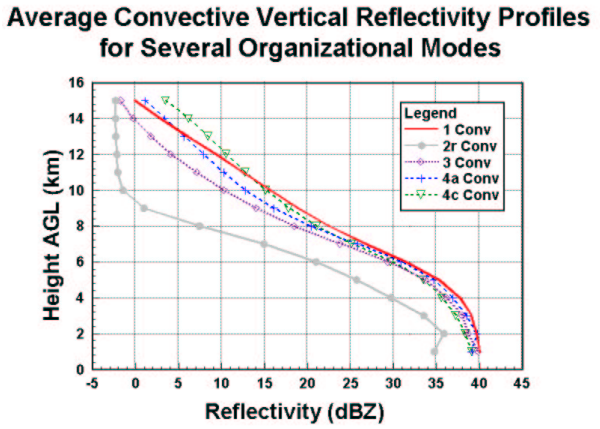

Figure 7: Averaged vertical profiles of radar reflectivity for convective regions from BMRC C-POL radar for Types **1**, **2r**, **3**, **3**, **4a**, and **4c**.

sions (**4c** in Fig. 6), consistent with recent simulations by Robe and Emanuel (2001). The origin and nature of these bands are uncertain, but their alignment approximately along the low-level shear vector makes boundary-layer rolls a candidate mechanism. This point was made for category **3** shear-parallel bands by LeMone et al. (1998). Also, the bands resemble pre-frontal lines observed at midlatitudes ahead of cold fronts (e.g., Trier et al. 1991). It is possible that weak downdrafts during this period prevented shear-perpendicular bands from developing. LeMone et al. did not observe similarly oriented low- and midlevel shear vectors (Type **4c**) in the TOGA COARE region, although LeMone (1983) did report such a case on 14 September 1974 in the eastern Atlantic during the GARP Atlantic Tropical Experiment (GATE). Several unclassifiable cases (**U** in Fig. 6) occurred throughout the period, some of which exhibited a variety of modes of organization within the radar domain. Over ten days from 16 to 25 May, 31 of the 40 six-hour periods (78% of the cases) were classifiable.

6. STRATIFORM RAIN FRACTION AS A FUNCTION OF ORGANIZATION

Averaged vertical profiles of radar reflectivity for grid points classified as convective for a number of the modes are shown in Fig. 7. The profiles are similar for all except the **2r** mode, which displays a much weaker reflectivity. This result is consistent with the observations for these cases showing much drier air aloft (Fig. 5) and hence shallower convective cells.

The following table summarizes convective classification results for all of the cases:

Type	STRAT AREA(%)	A%	STRAT RAIN(%)	R%
1	37	0.5	1	0.2
2	64	4.6	16	7.0
2r	43	5.6	9	3.2
3	78	42.7	36	41.1
4a	66	20.0	18	25.5
4b	59	4.2	9	3.0
4c	67	22.7	20	20.0
Total	69	100	25	100

In this table STRAT AREA refers to the areal percentage of stratiform rainfall, A(%) to the percent of the total area covered by each category, STRAT RAIN to the percent stratiform rainfall, and R(%) to the percent of the total rainfall for each category. Interestingly, the average percent stratiform precipitation for the entire period is rather small (25%), a value much less than the ∼40% often reported for the Tropics (Johnson and Houze 1987). However, this value is in good agreement with recent SCSMEX modeling results for the same period (Tao et al. 2003). Type **3** systems, which contribute the largest percentage of precipitation (41%), have the greatest percentage of stratiform rainfall (36%). The reasons for this behavior are not yet understood. The small percentage of stratiform rainfall from **2r** systems (9%), is consistent with the shallow character of these cloud systems (Fig. 7)

7. SUMMARY AND CONCLUSIONS

A preliminary analysis of radar data from the BMRC C-POL radar on Dongsha Island from 15 to 25 May, 1998 – a ten-day period following the onset of the East Asian summer monsoon over the northern South China Sea – reveals that lower and middle level vertical shears exert a dominant control over the structure and orientation of mesoscale convective systems in this region. The findings are consistent with those of LeMone et al. (1998) for TOGA COARE, except two new organizational modes have been identified: weak, shear-parallel bands (**2r** in Fig. 1) for strong low-level shear and weak midlevel shear when the air is dry aloft, and shear-parallel bands (**4c**) for strong shears in both layers when the shear vectors are in the same direction. Midlatitude influences likely contributed to these two additional modes by producing strong westerlies (in the case of **4c**) during the passage of a strong upper-level trough and midtropospheric drying (in the case of **2r**) following passage of the trough. The average stratiform rain fraction for the onset period (25%)

is much less than that reported for the Tropics as a whole (∼40%), but is consistent with the recent modeling results of Tao et al. (2003).

ACKNOWLEDGMENTS This research has been supported by the National Aeronautics and Space Administration under Grant NAG5-9665. We thank Paul Ciesielski, Tom Keenan, and Michael Whimpey for their assistance.

8. REFERENCES

Alexander, G. D., and G. S. Young, 1992: The relationship between EMEX mesoscale precipitation feature properties and their environmental characteristics. *Mon. Wea. Rev.*, **120**, 554–564.

Aves, S. L., and R. H. Johnson, 2003: The diurnal cycle of oceanic convection over the South China Sea during the Southeast Asian Monsoon. *Preprints, 10th Conf. on Mesoscale Processes*, Amer. Meteor. Soc.

Barnes, G. M., and K. Seickman, 1984: The environment of fast- and slow-moving tropical mesoscale convective cloud lines. *Mon. Wea. Rev.*, **112**, 1782–1794.

Chlond, A., 1988: Numerical and analytical studies of diabatic heating effect upon flatness of boundary layer rolls. *Beitr. Phys. Atmos.*, **61**, 312–329.

Christian, T. W., and R. M. Wakimoto, 1989: The relationship between radar reflectivities and clouds associated with horizontal roll convection on 8 August 1982. *Mon. Wea. Rev.*, **117**, 1530–1544.

Houze, R. A., Jr., 1977: Structure and dynamics of a tropical squall-line system observed during GATE. *Mon. Wea. Rev.*, **105**, 1540–1567.

Houze, R. A., Jr., 1982: Cloud clusters and large-scale vertical motion in the tropics. *J. Meteor. Soc. Japan.* **60**, 396–410.

Johnson, R. H., 1984: Partitioning tropical heat and moisture budgets into cumulus and mesoscale components: Implications for cumulus parameterization. *Mon. Wea. Rev.*, **112**, 1590–1601.

Johnson, R. H., and P. E. Ciesielski, 2002: Characteristics of the 1998 summer monsoon onset over the northern South China Sea. *J. Meteor. Soc. Japan.* **80**, 561–578.

Johnson, R. H., and R. A. Houze, Jr., 1987: Precipitating cloud systems of the Asian monsoon. *Monsoon Meteorology, X*, C.-P. Chang and T. N. Krishnamurti, Eds., Oxford University Press, 298–353.

Keenan, T. D., and R. E. Carbone, 1992: A preliminary morphology of precipitation systems in tropical northern Australia. *Quart. J. Roy. Meteorol. Soc.*, **118**, 283–326.

Kuettner, J. P., 1971: Cloud bands in the earth's atmosphere – Observations and theory. *Tellus*, **23**, 404–425.

Lau, K.-M., K.-M. Kim, and S. Yang, 2000: Dynamical and boundary forcing characteristics of regional components of the Asian summer monsoon. *J. Climate*, **13**, 2461–2482.

LeMone, M. A., 1973: The structure and dynamics of horizontal roll vortices in the planetary boundary layer. *J. Atmos. Sci.*, **30**, 1077–1091.

LeMone, M. A., 1983: Momentum transport by a line of cumulonimbus. *J. Atmos. Sci.*, **40**, 1815–1834.

LeMone, M. A., and R. J. Meitin, 1984: Three examples of fair-weather mesoscale boundary-Layer convection in the Tropics. *Mon. Wea. Rev.*, **112**, 1985–1998.

LeMone, M. A., E. J. Zipser, and S. B. Trier, 1998: The role of environmental shear and thermodynamic conditions in determining the structure and evolution of mesoscale convective systems during TOGA COARE. *J. Atmos. Sci.*, **55**, 3493–3518.

Moncrieff, M. W., and J. S. A. Green, 1972: The propagation and transfer properties of steady convective overturning in shear. *Quart. J. Roy. Meteorol. Soc.*, **98**, 336–352.

Robe, F., and K. A. Emanuel, 2001: The effect of vertical wind shear on radiative-convective equilibrium states. *J. Atmos. Sci.*, **58**, 1427–1445.

Rotunno, R., J. B. Klemp, and M. L. Weisman, 1988: A theory for strong, long-lived squall lines. *J. Atmos. Sci.*, **45**, 463–485.

Saxen, T. R., and S. A. Rutledge, 1998: Surface fluxes and boundary layer recovery in TOGA COARE: Sensitivity to convective organization. *J. Atmos. Sci.*, **55**, 2763–2781.

Steiner, M., R. A. Houze, Jr., and S. E. Yuter, 1995: Climatological characterization of three-dimensional storm structure from operational radar and rain gauge data. *J. Appl. Meteor.*, **34,**, 1978–2007.

Tao, W.-K., C.-L. Shie, D. Johnson, R. H. Johnson, S. Braun, J. Simpson, and P. E. Ciesielski, 2003: Convective systems over South China Sea: Cloud-resolving model simulations. *J. Atmos. Sci.*, (in press)

Trier, S. B., D. B. Parsons, and John H. E. Clark, 1991: Environment and evolution of a cold-frontal mesoscale convective system. *Mon. Wea. Rev.*, **119**, 2429–2455.

Tung, W.-W. and M. Yanai, 2002: Convective momentum transport observed during the TOGA COARE IOP. Part I: General features. *J. Atmos. Sci.*, **59**, 1857–1871.

Wentz F. J., C. Gentemann, D. Smith, and D. Chelton, 2000: Satellite measurements of sea surface temperature through clouds. *Science*, **288**, 847–850.

Wu, X. and M. Yanai, 1994: Effects of vertical wind shear on the cumulus transport of momentum: Observations and parameterization. *J. Atmos. Sci.*, **51**, 1640–1660.

Young, G. S., D. A. R. Kristovich, M. R. Helmfelt, and R. C. Foster, 2002: Rolls, streets, waves and more. *Bull. Amer. Meteor. Soc.*, **83**, 54–69.

Zipser, E. J., 1977: Mesoscale and convective-scale downdrafts as distinct components of squall-line circulation. *Mon. Wea. Rev.*, **105**, 1568–1589.